EEET ECOLOGICAL ENGINEERING & ENVIRONMENTAL TECHNOLOGY

Ecological Engineering & Environmental Technology, 2025, 26(4), 13–33
https://doi.org/10.12912/27197050/200492
ISSN 2719–7050, License CC-BY 4.0

Received: 2024.01.16
Accepted: 2025.02.15
Published: 2025.03.01

Novel deep learning training optimizer issues analysis to detect seashore high and low tides

Gopi Vadapalli[1], Rajesh Duvvuru[1*]

[1] School of Computer Science and Engineering, VIT-AP University, Amravathi, India
* Corresponding author's e-mail: dr.rajeshduvvuru@gmail.com

ABSTRACT

High tide causes rip waves that causing disruptions and deaths in beaches of India and rest. In most of the beach drowning deaths are rising due to a lack of early warning information. Currently beach guards need real-time beach monitoring tide warning systems to rescue drowning people. While deep learning technologies excel at predicting objects, they struggle to accurately forecast high and low tides information for beach swimmers. At present the high and low tide detection accuracy is lower, due to that the early warning system are not functioning effectively. To improve the tide detection efficiency the dataset training must achieve higher accuracy. This paper addresses deep learning training issues to improve novel tide dataset training accuracy with novel tide dataset. This study suggests the best deep learning training network for beach tide classification. The work fine-tunes optimizers and epochs to look at the modern deep learning algorithms ResNet-18 and ResNet-50. This study tests deep learning training networks namely, RMSProp, SGDM and ADAM with epochs starting from 30 to 500 and applies three optimizers to balanced tide data. When using SGDM at shorter epochs, ResNet-18 and ResNet-50 achieved 100% training accuracy. The ResNet-50 training network had 100% classification accuracy with all three optimizers in lower and upper epochs. ResNet-50 integrated with SGDM and ADAM optimizers obtained 100% success at reduced epochs compared with ResNet-18. The present study examines only two training classes, i.e., high and low tides, and it can be extended by adding a few more object classes like humans and ferries. This unique approach aids in automating smart beach monitoring devices, enabling them to continuously send out high and low tide alerts using ResNet-50. The dissemination of tide information is crucial for rescue operations to prevent drowning cases and reduce fatalities in Indian and rest beaches.

Keywords: deep learning, CNN algorithm, beach, high-tide, low-tide.

INTRODUCTION

India has 7,516.6 miles of mainland and island coastline. East, south, and west are the Bay of Bengal, Indian Ocean, and Arabian Sea. India is a maritime nation with popular beaches for leisure activities [Ramakrishna et al., 2010]. The coastline environs in India can also be dangerous due to large waves, violent currents, shifting tides, and complex and ever-changing physical features [Mehta et al., 2019]. The WHO predicts 236,000 drowning deaths in 2019. In 2019, injuries caused nearly 8% of deaths. Drowning is the third leading cause of unintentional injury deaths at 7%. The inaugural regional evaluation on drowning prevention by the World Health Organization (WHO) reveals that in 2019, a staggering 144,000 individuals lost their lives due to drowning in the Asia Pacific area alone, constituting a significant 61% of the total global drowning fatalities [Ray-Bennett et al., 2024]. The report was published prior to World Drowning Prevention Day on July 25th. It indicated that drowning resulted in the deaths of approximately 70,000 to 74,000 individuals in South-East Asia and the Western Pacific region. Between 2020 and 2023, 38,000 beach drowning occurred. Beach-related drowning in India is a chronic issue because to its social, economic, and emotional effects. Most drowning deaths in India occur in the northeast, followed by Andhra Pradesh and Maharashtra, according to the report. Rip currents have killed 39 Indians annually during the past decade. The east coast

of India had 30–40 drowning each year, while the west coast had 5–10 [Ravimuni,et al., 2022]. Rip currents killed around 350 people in coastal Andhra Pradesh, saving only 10. Although inconsistent, the powerful rip current that causes most drowning deaths in the state forms during high tides. It operates 50–150 feet and suction force can reach five to eight kilometers per hour, making beaches dangerous. According to the National Crime Records Bureau (NCRB-2019) survey reports, the state of Andhra Pradesh recorded 1,554 fatalities due to drowning. Out of the total deaths, 44% were classified as accidents, while the remaining deaths were attributed to suicides and other reasons. The present work especially concentrates on the high-tide causing deaths that are very high in the state of Andhra Pradesh and rest of the India. Many such incidents were recently reported and that are as follows: Annually, around 1,500 individuals succumb to drowning in the state of Andhra Pradesh. Between 2017 and 2021, Andhra Pradesh recorded a total of 8,299 drowning fatalities.

The drowning statistics show that throughout the course of the past twelve years, there have been a total of more than two hundred people who have lost their lives as a result of drowning accidents that have occurred at a variety of beaches in and around Vizag. Several beaches, including RK Beach, Bheemili Beach, Rushikonda Beach, and Yarada Beach, have become dangerous places to visit. There were a total of sixty people who passed away at RK beach during the years 2016 and 2022, as indicated by the given data. There were a total of thirteen people who lost their lives at the beach as a result of drowning during the years 2017–2021 (Fig. 1).

Currently, a smart beach high-tide system is required to alert swimmers inside the beaches of India and the rest of the world. At present the Indian lifeguards manually patrol beaches from a tower. They warn people against entering rip current or high-tide zones through speaker announcements. Manual monitoring incurs significant costs and delays the identification of high tides or rip currents, potentially causing damage to beach swimmers and even resulting in fatalities. The present beach monitoring and alert systems (BMAS) target water quality, erosion, bacteria, debris, marine litter, and waste management [Halliday et al., 2011; Liu et al., 2024; Little et al., 2022; Pikelj et al., 2018]. Hazard-based BMAS, especially rip current and high tide monitoring, lacks resources. The field of computer vision has done a lot of research on using deep neural networks to find objects. But most tests and studies are focused on finding real things such as humans, vehicles, places etc., and there are clear lines between what is and isn't an object [de Silva et al., 2021]. Identification of High tides is transient phenomena that are not visible in every instance and lack well defined boundaries, even when they can be observed. The applicability of present approaches remains uncertain. Deep learning models are now better at finding high-tides than present machine learning models. Even fewer researchers tried to achieve fine detection accuracy, but still it is big challenge in identifying the high-tide due to limitations in tide dataset, optimizer and epoch selection.

This study aims to integrate deep learning technologies for the identification and monitoring of tidal waves in Bay-of-Bengal-like coastlines, where the detection accuracy for multi-class tidal waves is inadequate. Object detection accuracy is mostly contingent upon training precision; yet, researchers frequently encounter uncertainty regarding the optimal configuration of hyperparameters, including learning rate, epochs, and optimizers,

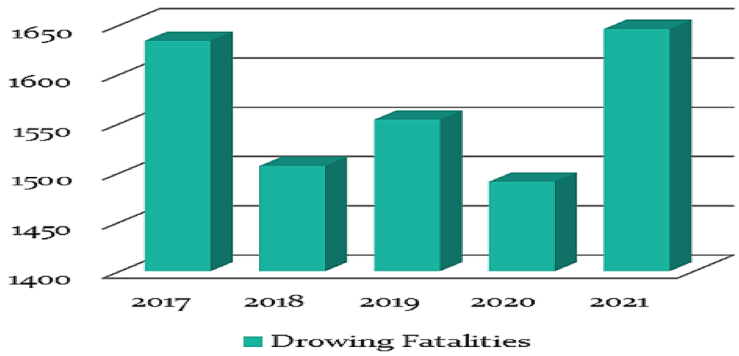

Figure 1. Drowning fatalities reported in the state of Andhra Pradesh during 2017–2021. National Crime Records Bureau (NCRB-2022)

to attain 100% accuracy. To improve accuracy, consider data properties and class count when choosing a training network. The current study enhanced training accuracy on a novel custom tidal dataset using ResNet-18 and ResNet-50 two popular pre-trained models. This research used 110 raw-tide images of Bay-of-Bengal beaches located in Andhra Pradesh state. We operated each training network independently while maintaining uniformity in all other hyperparameters (such as epochs, optimizers, learning rate, etc.). The optimizers namely SGDM, ADAM, and RMSProp are adjusted for 30–500 Epochs the ResNet-18 outperformed ResNet-50. The SDGM, ADAM, and RMSPROP helped ResNet-18 train categorization with 89.74% accuracy. However, ADAM outperforms SGDM and RMSPROP almost for majority of iterations. To improve training accuracy in balanced Tide datasets, this study found the best deep learning network, optimizers, and Epoch rate. This study compares ResNet-18 and ResNet-50 highest training accuracy on tidal dataset. A very limited study was carried out in the areas of beach tides detection using deep learning. This study uses tide datasets to find the best hyper-parameters for training accuracy of ResNet-18 and ResNet-50. The ResNet-50 looks to be the best network for detector algorithms based on dataset training outcomes. Deep learning models now outperform conventional approaches in rip current detection. Due to poor data dispersion, these models still have accuracy limits. Most studies have focused on human detection close and inside beaches and very strong waves. This study will monitor beach conditions for swimming by identifying high and low tides that can trigger rip currents. Deep learning systems now recognize objects with astonishing precision.

Advanced deep learning algorithms like Autoencoders, CNNs, SOMs, DBNs, LSTMs, RBFNs, RNNs, GANs, MLPs, and RBMs can detect objects with varying degrees of accuracy [Girin et al., 20]. Recently, CNNs have excelled at multiclass object detection [Mohana et al., 2021]. Presently, maritime tide prediction endeavors have progressed markedly, integrating elements such as high-tide and low-tide, while employing the Internet of Things (IoT) and artificial intelligence (AI) to alert the public regarding drowning incidents. At present, AI-driven deep learning technologies are pivotal in object prediction; yet, their precision in forecasting sea tide waves remains comparatively inadequate. In deep learning algorithms, the training of networks, along with optimizers and epochs, is essential for attaining greater accuracy in object detection. Currently, there is a necessity to advance smart artificial intelligence technologies that can effectively notify citizens and local authorities to commence prompt rescue operations. Identifying high-tide and low-tide waves presents a considerable problem, especially at hazardous beaches. The accuracy of tidal wave detection presents a considerable challenge for academics and practitioners, as enhanced detection accuracy largely relies on the training accuracy of the image collection. Nevertheless, researchers have performed few pre-training tests to evaluate the efficacy of Tide detections. Typically, high training accuracy may lead to superior test accuracy. Notwithstanding the network training model's acclaim for object detection, the Epoch rate for optimal data training is still to be determined.

The current research only trains problems using Tide datasets and needs be tested for accuracy using detector algorithms like YOLO, MobileNet, etc. ResNet-50 is better in training Tide datasets related with water photos, according to this study. This technical analysis helps the Indian Coast Guards (ICG) and Marine Police (MP), which has few tidal facilities. These sorts of deep learning approaches for tide datasets are useful to transmit location information and early warnings periodically, which could detect high tides and result in a lower fatality rate on Indian beaches. The rest of the paper is organized is as follows: Section two sets the framework for our inquiry by evaluating relevant literature and technique. Section three explains our new strategy. Section four details our research plan to attain our goals. Section five details our findings on the proposed technique, its efficacy, and its effects. Lastly, section six summarizes our main findings and suggests additional research.

Related works

Artificial intelligence-based beach wave detection has reduced risk and saved lives from rip currents and high tides. An AI model by Shimada et al. can detect rip currents near the jetty. A single AI model identified flash rip currents in open areas and stationary rip currents near jettys. Training the AI model under various conditions allowed us to reliably detect rip currents at each location [Shimada et al., 2023]. Najafzadeh et al. calculated the RTR for 50 southern Chinese beaches using nine Machine Learning

(ML) models for RIP wave recognition. ML models include M5 Model Tree (MT), AdaBoost, MARS, SVM, EPR, GEP, Stacked, XGBoost, and Random Forest (RF). This strategy produced a reliable southern Chinese coast study dataset. The study forecasts rip current vulnerability using two parameters: Ω (dimensionless fall velocity) and TR (tide range). During training and testing, R, RMSE, violin diagrams, heatmaps, and Taylor diagrams analyzed AI model performance. Therefore, MARS predicted RTR better than other AI algorithms. Results showed RTR estimation's accuracy and effectiveness. To protect beachgoers, Southern Chinese beach operators must aggressively manage high tides and high rip current danger [Najafzadeh et al., 2024]. studied Parangtritis beach's cove-shaped coastline morphology. ALOS PALSAR images were used to determine the surf zone and breaking waves. Others have used the Radon Transform for wave runup video motion detection, comparing it to color contrast from RGB photographs and LiDAR measurements [Almar et al., 2017]. The study on 'high-tide' detection that produces beach rip currents is sparse. Koon et al. explored an association between tide patterns and fatal drowning at New South Wales surf beaches. Their research informs coastal safety management and practice. First, high tide can cause non-swimmers and young children to slip into deep water [Puleo et al., 2016]. Tides effect surf-zone wave-breaking, which creates rip currents. Tidal currents can affect tidal inlets, coastal engineering constructions, and beach nourishment areas more than open-ocean beaches [Yadhunath et al, 2022]. As the tide rises in coastal areas with rough beaches, straits, offshore pressures, huge tidal ranges, and offshore islands, can interact with approaching waves to raise breaking wave heights Tides' influence on rip current flow behavior, especially wave breaker patterns, are crucial for swimmers and bathers' safety on beaches with rip currents and high-tides [Koon et al., 2023]. Due to the criticality of identifying high tides, limited high-tide detection studies with higher accuracy are available in AI literature [Vitousek et al, 2023]. Currently there is a need to create a beach monitoring system for the safety of beach visitors; using optimal image sensing is more challenging, especially working with deep learning technologies [George et al., 2024]. Moreover selection of right deep learning optimizer to attain higher accuracies is more critical challenge ahead for the tidal images [Elshamy et al., 2023; Lambu et al., 2024].

Study area

The real-time tide dataset is collected from four drowning and high-tide zone beaches of Andhra Pradesh state, India. The four high-tide vulnerable beaches are Rama Krishna beach (RK Beach) (17° 42' 51.4584'' N, 83° 19' 25''), Pudimadaka beach (17° 29' 24'' N, 83° 00' 13''), Manginapudi beach (16° 14' 37'' N, 81° 14' 26'') and Surya lanka beach (15° 50' 55'' N, 80° 32' 01''). Figure 2 shows the geographical locations of the high-tide zone beach of the study area in the state of Andhra Pradesh. Andhra Pradesh is in the Northern hemisphere region on

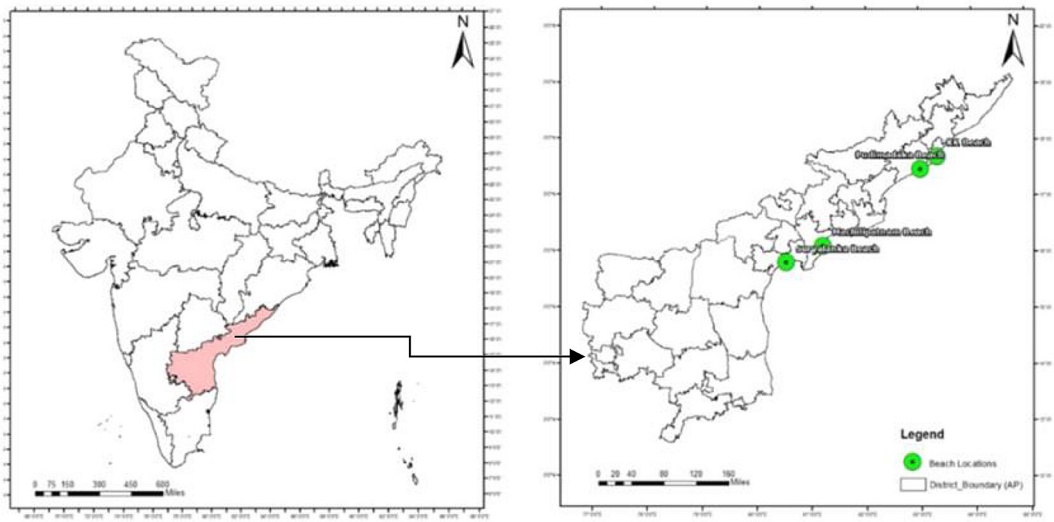

Figure 2. Location map of the study area

the southeastern coast of the Indian Peninsula in the Bay of Bengal (Fig. 2). Andhra Pradesh, known as the "Sunrise state of India" for its coastline tourism, has nine seaports. Andhra Pradesh possesses the second-longest coastline in India, extending 975 km that covers nine major seaports along the Bay of Bengal. The recent drowning statistics of Drowning killed 8,299 Andhra Pradesh residents from 2017 to 2021, it reflects that almost every year 1600 drowning deaths are recorded every year. Especially over the past 12 years, 200 people have drowned at Visakhapatnam district beaches. The drowning statistics also specified that, 60 people drowned at RK beach during 2016–2021. This beach is the most vulnerable to rip currents and high-tides, which killed 92 surfers from 2000 to 2010. Rip currents and high-tides were also found in Surya Lanka and Manginapudi beaches (Fig. 3). Figure 3 shows field pictures at different locations of the study area beaches such as location (A) RK Beach near Visakhapatnam district; (B) Pudimadaka Beach near Anakapalli district; (C) Manginapudi beach near Machilipatnam city; (D) Suryalanka beach near Bapatla district.

The RK Beach became popular after independence because Vizag's public and private sector enterprises attracted a huge workers, their families, and tourists. The natural harbor and Visakhapatnam Port in the 1930s boosted the region's economy, enabling tourism. Indians and foreigners visited the long untouched seashore for its beauty. The submarine museum, clean waterways, and Bay of Bengal view were main attractions. The aquarium here is an added attraction. The sea's roar is wonderful. Tourism at RK Beach flourished in the 20th century as Vizag became a port city (Fig. 3A).

Pudimadaka Beach on the Bay of Bengal ranks 35th of 115 Andhra Pradesh beaches. Capital city Amaravathi is 302 kilometers away and situated in Anakapalli district. Pudimadaka, the nearest town Anakapalli, is 0.1 km from the beach. The gorgeous Bay of Bengal coast has this kilometers-long sand beach. Since the bottom gradually shrinks, aqua socks are unnecessary. Pudimadaka Beach is unspoiled by services. The beach is popular with tranquil resters (Figure 3B). In Krishna District, Andhra Pradesh, Manginapudi Village has the beautiful Manginapudi Beach. It borders the Bay of Bengal on the shore. Machilipatnam, a popular tourist site, lies 15 km from the seashore. Other local landmarks include Manginapudi Beach, 80 km from Viajayawada, 82 km from Eluru, and 117 km from Guntur. Visakhapatnam (Vizag), a prominent state holiday resort, is 340 km from this beach. The famed Manginapudi Beach in Andhra Pradesh is a great beach vacation spot. It is also called Machilipatnam Beach and Bandar Beach locally. All pathways lead to Manginapudi Beach, despite its many names. Beautiful vistas, reasonable accommodations, and local activities draw tourists to the beach. The area's unique feel is perfect for anyone seeking a break from their busy lives (Figure

Figure 3. Study area beaches: (A) RK beach located in Visakhapatnam district; (B) Pudimadaka beach located in Anakapalli district; (C) Manginapudi beach located in Krishna district; (D) Suryalanka beach located in Bapatla district of Andhra Pradesh, India

3C). Suryalanka beach, 8 km from Bapatla town, Andhra Pradesh, offers a peaceful escape on the Bay of Bengal. Weekends and vacations are ideal for relaxing at Bapatla beach. Natural splendor of flowing waves invites strolls and picnics (Fig. 3D).

Methodology

Methodology is shown in Figure 4, it focuses majorly on shows data acquisition, pre-processing, training of tidal data, deep convolution neural network (DCNN), Classifier, train the of tidal data for best detection of high-tide and low-tides. The DCNN comprises with two popular pre-trained ResNet-18 and ResNet-50 networks for validation of best training analysis to find high-tide.

Raw tide data collected

The gravitational influence of the moon on Earth is a crucial factor in the formation of tides. The gravitational attraction between two objects increases as their proximity to one other diminishes. Although both the sun and the moon exert gravitational forces on Earth, the moon's influence is considerably stronger due to its proximity to the Earth compared to that of the sun. The moon exemplifies a tidal force due to its ability to elevate the tides on Earth. The moon exerts a tidal influence on the entire planet. The diminished flexibility of Earth's terrestrial surfaces renders them largely unaffected by this. Nonetheless, within a single day, terrestrial surfaces can shift up to 55 centimeters (22 inches) in either direction. Terrestrial tides refer to these movements. Terrestrial tides can modify the exact location of an object. In radio astronomy and the determination of coordinates using a global positioning system (GPS), terrestrial tides are critically important. Volcanologists study terrestrial tides because the movement of the Earth's crust can occasionally trigger a volcanic eruption. The tidal force exerted by the moon significantly influences the ocean's surface. As a liquid, water has a heightened responsiveness to gravitational forces. Tidal range refers to the vertical disparity between high tide and low tide. The gravitational influence of the sun on Earth results in a monthly shift in the range. Despite being nearly 390 times further distant from Earth than the moon, the sun's mass influences tides.

High-tide

The hemisphere of the Earth oriented towards the moon experiences the highest tidal force exerted by the moon. On the side of the Earth that is oriented away, it is in its most vulnerable state. The ocean's capacity to bulge outward simultaneously at two distinct areas is facilitated by variations in gravitational force. When the Earth is oriented towards the moon, a bulge is observable on that side.

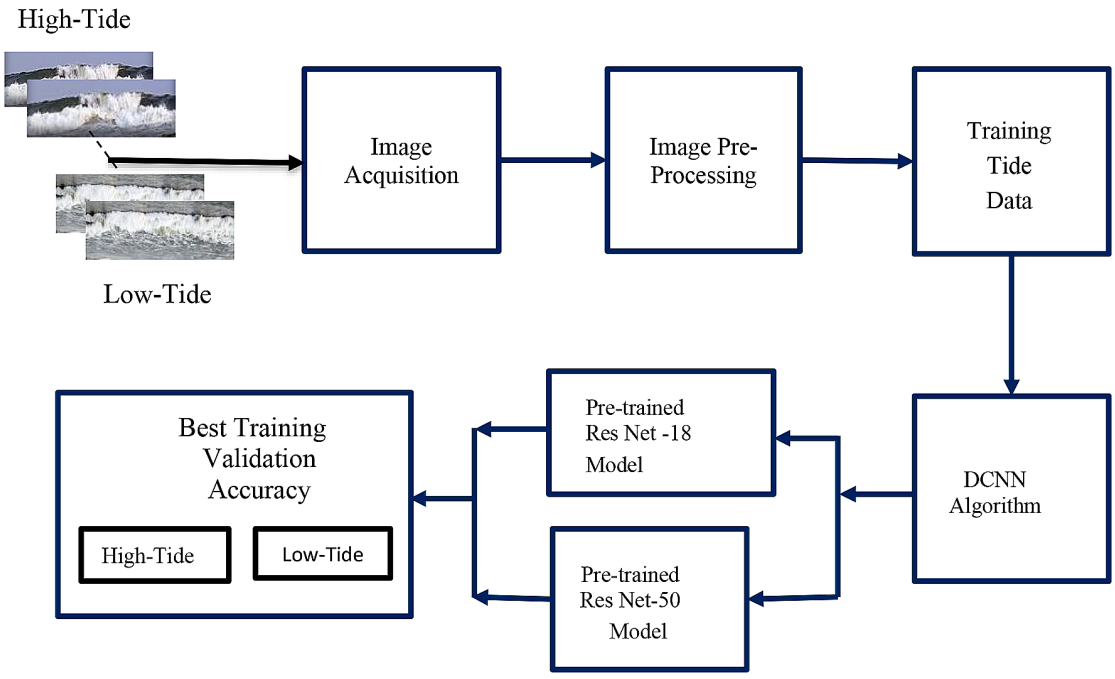

Figure 4. Proposed high-tide detection methodology

This is the direct tidal force exerted by the moon, which is attracting the ocean towards it. One bulge is situated on the Earth's opposite side from the other. From this perspective, the sea protrudes away from the moon. One possible interpretation of the bulge is that it is the tidal force of the moon that is dragging the planet (and not the water) toward it. The term "high tide" refers to these bulges that occur in the waters of the ocean. It is referred to as the high tide when the tide is at its highest on the side of the Earth that is facing the moon. A low high tide is the name given to the high tide that is brought about by the bulge that is located on the opposite side of the Earth. When the ocean is open, the water pushes outward in the direction of the moon. The water rises and stretches out onto the land along the coastline with the tides. As per the Tides data 2024, the height of the high tide in the study area differed. Among the four beaches in the study area, RK Beach and Pudimadaka Beach recorded almost similar tide heights. The average height ranges from 0.96 meter to 1.83, and the average high-tide height is 1.395 m per day. In contrast to RK and Pudimadaka beaches, the high-tide heights at Manginipudi and Suryalanka beaches are nearly identical. The high-tide heights in Manginipudi and Suryalanka beaches range from 0.88 m to 1.65 m, with an average high tide height of 1.265 m. The high-tide statistics reveal that the tides at RK and Pudimaka beaches average 0.13 m higher per day than those at Munginipudi and Suryalanka beaches. We also observed that the distance between beaches played a crucial role in recording the similar high-tide values between the RK and Pudimadaka beaches, which also reflected similarly in the Manginapudi and Suryalanka beaches. Figure 5 represents the sample images of high-tide class in the novel tide dataset with 50 MP resolution each and Figure 6 presents the high-tide information for the study area beaches over a period of four months (September to December).

Figure 5. Dataset of high-tide images

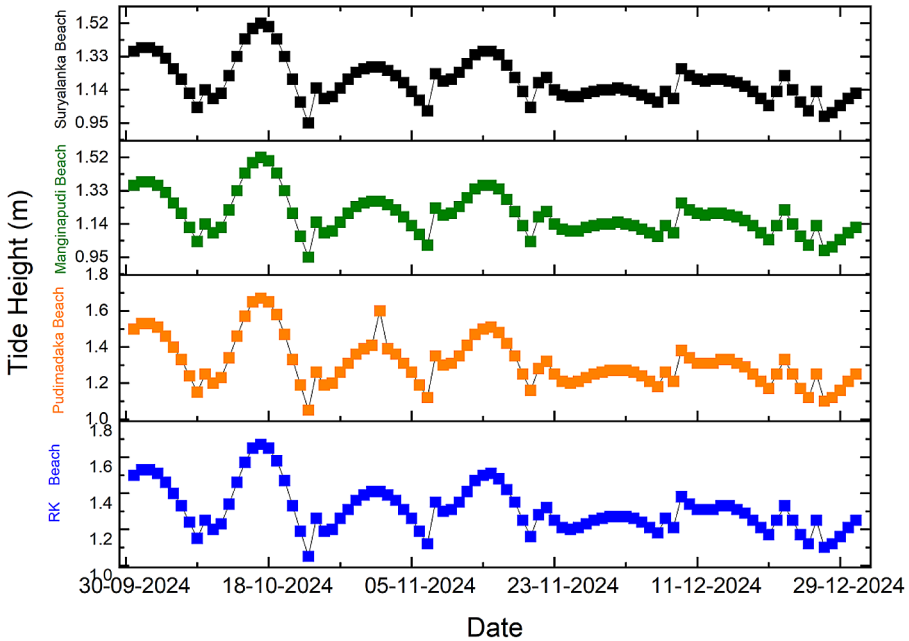

Figure 6. Height of the high-tides in the study area (RK beach, Pudimadaka beach, Manginapudi beach, Suryalanka beach). Tide charts, (http://www.tideschart.com/india/andhra-Pradesh/)

Low-tide

Tidal range and frequency are influenced by the geography of the seacoast and ocean floor. Water has the potential to disperse extensively on a polished and wide beach. The tidal levels can fluctuate by a few millimeters. In a relatively narrow, rocky entrance or harbor, the tidal range may extend over several meters. Low tide is characterized by the minimum elevation or lowermost point of the wave. The low-tide are safe for the people to swim and enjoy. The low-tide data set is collected from all four beaches of the Andhra Pradesh state with 50 MP image resolution (Fig. 7).

The tides data for 2024 indicate variability in the height of low tide within the study area. RK Beach and Pudimadaka Beach exhibited comparable tide heights among the four beaches in the study area. The average height varies between 0.02 meters and 0.75 meters, with a daily average low-tide height of 0.385 meters. The low-tide heights at Manginipudi and Suryalanka beaches are nearly identical, in contrast to those at RK and Pudimadaka beaches. The low-tide heights at Manginipudi and Suryalanka beaches vary from 0.01 m to 0.69 m, with an average of 0.35 m. The low-tide data indicate that the tides at RK and Pudimaka beaches are, on average, 0.035 m lower per day compared to those at Munginipudi and Suryalanka beaches. The distance between beaches significantly influenced the comparable low-tide values observed at RK and Pudimadaka beaches, a trend that was also evident at Manginapudi and Suryalanka beaches. Figure 8 illustrates the low-tide data for the study area beaches across a four-month duration, from September to December.

Dataset

The novel tide dataset contains 322 tide photos divided into hide-tide (175) and low-tide (142). The beaches in the research region are captured using a high-resolution Nikon D-850

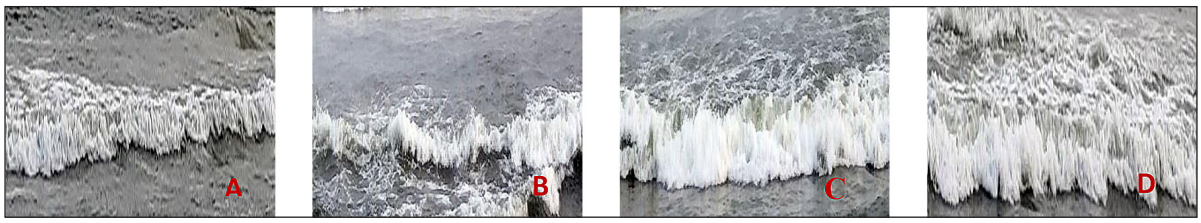

Figure 7. Dataset of low-tide images

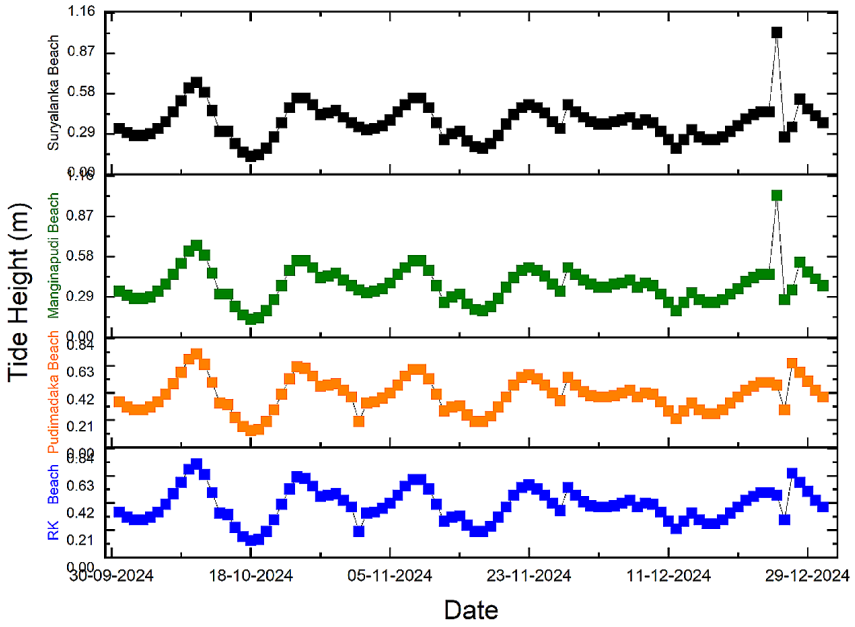

Figure 8. Height of the low tides in the study area (RK beach, Pudimadaka beach, Manginapudi beach, Suryalanka beach). Tide charts, (http://www.tideschart.com/india/andhra-Pradesh/)

camera, which has a resolution of 45.7 megapixels. The data undergoes pre-processing to ensure a high-quality dataset. Pre-processing removes distortions and improves essential aspects. We preprocess the dataset using these methods:

The data profiling was conducted on the raw tide dataset, focusing on shuffling, size, color, and brightness. The open-source 'Data Gradients' tool profiles Tide datasets by focusing on various picture quality factors such convexity, fine details, segments, brightness and color distribution, aspect ratios, and resolution.

The data cleaning involved the removal of redundant, incorrect, improperly, corrupted, blur, formatted, or incomplete tide images. We collected 105 high-tide images and removed 70. We removed 38 of 142 low-tide photos, most of which are duplicates and few are indistinct [Meliboev et al., 2022]. Classifying balanced datasets is more accurate and less prejudiced than imbalanced datasets.

The image enhancement process included the meticulous selection and resizing of 209 high-resolution tidal wave photographs to dimensions of 640 × 640 pixels for the present study across each class [Li et al., 2021]. (IV) The Tides class images are subjected to an eight-fold augmentation process, resulting in a total of 4471 images. The dataset is rotated clockwise, counter-clockwise, upside-down at 90°, and two times at -15° and 15°. Blurring, noising, horizontal and vertical flips, and angle flipping (Kumar et al., 2024). We allocate seventy percent for training, ten percent for testing, and twenty percent for validation from the dataset (Fig. 9–H).

The mathematical notations and assumptions

The classification of tide disease is executed on the feature map function. The feature map f(h) is the product of the input (α) and the kernels (β).The feature classification function is specified in Eq. 1.

$$f(h) = (\alpha * \beta)(h) = \sum_{l=-\infty}^{l=\infty} \alpha(x) \bigcup (x + h) \quad (1)$$

where: x denotes the array of tide samples that spans from negative infinity to positive infinity, h denotes the feature map, while α represents the input.

EXPERIMENTATION

The deep convolution neural network architecture

The tide classification experimentation is done on Matlab computer vision platform. The Convolutional neural networks (CNN) are a prevalent deep learning technique that requires substantial training of multiple layers. The CNN can be employed to create a computer model that processes chaotic image inputs and transforms them into suitable classification output categories (Fig. 10).

Tide dataset training process

The tide dataset is trained on two different types of ResNet deep convolution neural networks. The two network layers commonly consists of layers such as Input layer, Softmax layer, Global Average

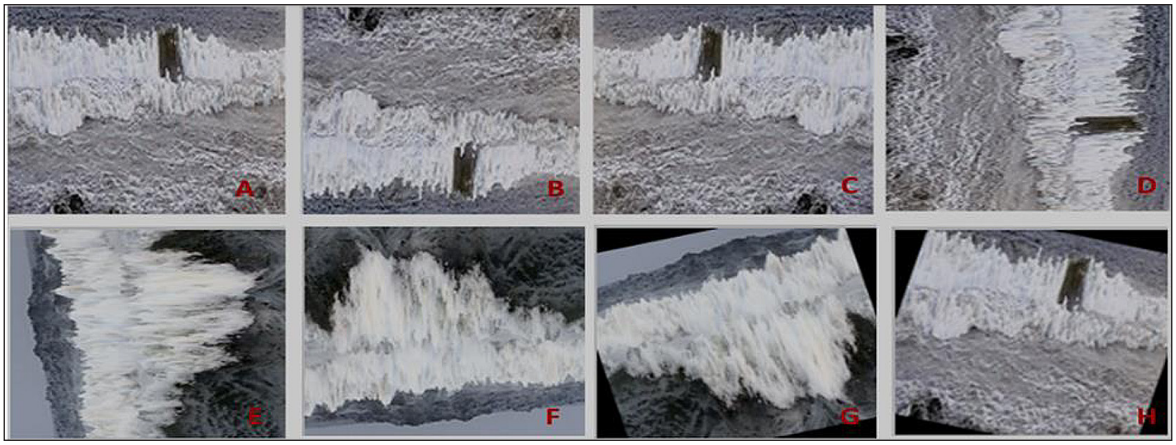

Figure 9. Eight-fold augmentation dataset of high-tide (A) Original high-tide image; (B) Flip (horizontal); (C) Flip (vertical); (D) Rotation (90° – clock-wise); (E) Rotation (90° – clockwise); (E) Rotation (90° – counter clockwise); (F) Rotation (90° – upside-down); (G) Rotation (-15°); (H) Rotation (15°).

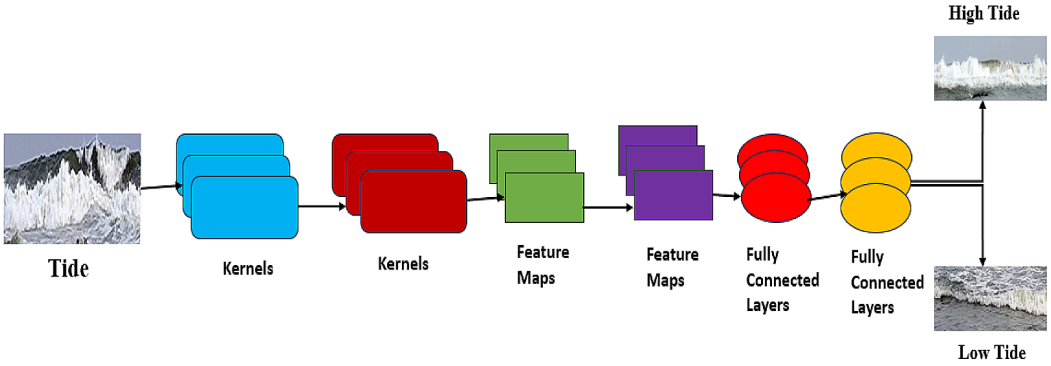

Figure 10. The ResNet-based CNN Tide classification system architecture

Pooling 2D layer, ReLU layer, fully connected layer, maxpooling layer, convolution 2D layer, etc., and the detail discussion is as follows (Fig. 11).

Deep convolution ResNet-18 architecture

The 71 layers of the ResNet-18 architecture are used to train the classifier on the created Tide dataset. The ResNet-18's comprehensive training architecture is shown in Figure 5. The layers in Figure 6 are as follows: 20 layers for Batch Normalization, 20 layers for convolution, 17 layers for ReLu, 8 layers for addition, Image input, Max pooling, softmax, 2-D global average pooling, fully connected, and classification output. 20×20×17×8 may be used to design the overall architecture of when utilizing Deep Neural Networks to train the data (Fig. 9 and Table 1).

Image input layer

Typically, the network receives an input picture with dimensions of 224×224×3, where 224×224 stands for the spatial dimensions (height and width) and 3 for the RGB color channels.

SoftMax layer

The Integer, or collection of Integers, serves as the axis for the SoftMax normalization, maintaining the same dimensions as the input. The SoftMax function serves as an activation function.

ReLu layer

Each input element undergoes a threshold operation via a ReLU layer, which nullifies any value below zero. The layer characteristic values in this instance include a negative slope greater than or equal to zero, a threshold value, and a maximum value.

Addition layer

The standard dropout probability is 0.5. The dropout layer randomly assigns input items a value of zero with a predetermined probability.

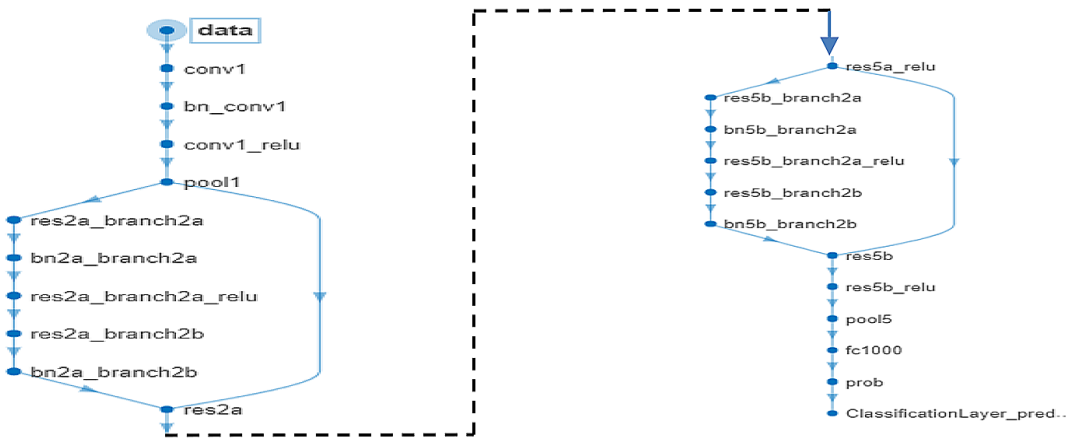

Figure 11. Internal deep learning ResNet-18 architecture

Global average pooling 2D layer

The downsampling is executed by the average pooling operation layer, which partitions the input into pooling regions and computes the average value for each area, encompassing the layer's height and width dimensions. This layer contains a single output.

Fully connected layer

The output value in fully connected layer is two, whereas the input dimension is configured to auto. Moreover, the BiasL2Factor is considered 0 when the values of the bias learn rate factor WeightL2Factor, and weight learn factor, are all set to 1. Next, the Glorot and zeros processes of the weights initializer and bias initializer, respectively, were started.

Max pooling layer

The components of the Max Pooling layer are padding, strides, and pool size. When training an integer or tuple of three integers, the greatest value should be taken across a certain window size. The maximum value across a 3×3 pooling window will be taken by (3, 3). The padding is defined as (0, 0, 0, 0) and the steps that the pooling window travels for each pooling step.

Convolution 2D layer

Basic characteristics of the convolution 2D layer are filter size (3, 3), number of filters (64), Stride (2, 2), and dilation factor (1, 1). Furthermore, the weights single are 33×3×64 and the padding value is ‚0'. Bias single is thus 1×1×64. Additional weight settings include BaseL2Factor as „0", weights initializer as „glorot", and base initializer as zeros. Additionally, weight learn rate factor, Weight2Factor, or bias learn rate factor may be set to 1 and rest.

Batch normalization layer

The Batch Normalization Layer's convolution, the output is normalized using a batch normalization layer, which improves training stability and speeds up convergence.

Classification output layer

The two tidal classes that are in need of classification are high tide and low tide, and they are both contained within the classification layer, which is the specified output layer. Cross-entropy is the loss function, and the output size is two.

Deep convolution ResNet-50 architecture

The 177 layers of the ResNet-50 architecture are used to train the classifier on the created Tide dataset. The ResNet-50's comprehensive training architecture is shown in Figure 5. The layers in Figure 6 are as follows: Image input layer, 2-D global average pooling layer, 53 batch normalization layers, 53 convolution layers, SoftMax layer, max pooling layer, fully connected layer, 49 ReLu layers, 16 addition layers, and classification output layer. 53×53×49×16 may be used to design the overall architecture of when employing deep neural networks for data training (Fig. 11 and Table 1).

Image input layer

Typically, the network receives an input picture with dimensions of 224×224×3, where

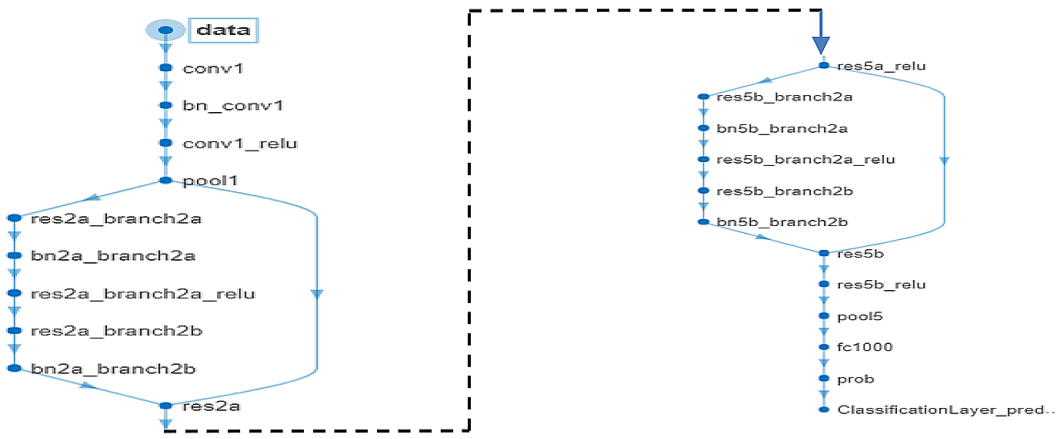

Figure 11. Internal deep learning ResNet-18 architecture

Table 1. ResNet-18 CNN layers (71)

S.No.	Name	Type	Activations (S × S ×C×B)	Learnable properties
1	Data 224×224×3 images with z 'score' norms	Input image	224× 224 ×3×1	–
2	Conv1(64 7×7×3) convolutions with stride [2 2] and padding [3 3 3 3]	Convolution	112×112×64×1	Weights (7×7×3×64) Bias (1×1×64)
3	bn_conv1(64)	Branch normalization	112×112×64×1	Offset 1×1×64 Scale 1 ×1×64
4	Conv1_relu	ReLu	112×112×64×1	–
69	Fc1000	Fully connected	1×1×1000×1	Weights 1000×512 Bias 1000×1
70	Prob Soft max	Softmax	1×1×1000×1	–
71	Classification Layer_predictions Cross entropy ex with 'tench'	Classification output layer	1×1×1000×1	–

224×224 stands for the spatial dimensions (height and width) and 3 for the RGB color channels.

SoftMax layer

The integer, or group of integers, is used as the basis for the SoftMax standardization, keeping the same size as the input. The SoftMax function is used as an activation function.

Global average pooling 2D layer

On average in order to decrease feature maps' spatial dimensions (width and height) while keeping important information, pooling is often used. An input (such a feature map from a convolutional layer) is sent into the pooling layer, which splits it into pooling regions (like 2×2 or 3×3 blocks) and finds the average value within each area. The input is then compressed or down-sampled as a consequence.

Addition layer

The dropout layer randomly changes some input elements to zero with a specific chance, and the usual chance is 0.5.

ReLu layer

An operation known as a threshold operation is carried out on each element of the input by a ReLu layer. This operation sets to zero any value that is less than zero. There are values for the layer characteristics that are higher than or equal to zero, including the max_value, the threshold value, and the negative slope.

Fully connected layer

The output size in this layer is set to two, and the input size is set to auto. Furthermore, only the BiasL2Factor is regarded as 0 when the other parameter values, Weight Learn Factor, WeightL-2Factor, and Bias Learn Rate Factor, are set to 1. Next, the processes for WeightsInitializer and Bias Initializer were started with zeros, respectively.

Max pooling layer

The max pooling layer comprises pool size, strides, and padding. in training, an integer or a tuple of three integers specifies the window size for determining the maximum. (3, 3) will extract the maximum value from a 3×3 pooling window. An Integer, a tuple comprising two integers, or none. The Strides parameter indicates the distance the pooling window advances with each step, configured as (2,2), with padding set to (0,0,0,0).

Convolution 2D layer

The convolution 2D layer has fundamental attributes such as a filter size of (3,3), a quantity of 64 filters, a stride of (2,2), and a dilation factor of (1,1). Additionally, the padding value is set to '0', and the weights are specified as 3×3×3×64. The bias single measures 1×1×64. Furthermore, supplementary weight parameters include weight learn rate factor, Weight2Fact, and bias learn rate factor set to 1, while the BaseL2Factor is designated as 0, weights initializer is defined as glorot, and base initializer is established as zeros.

Classification output layer

There are only two tidal classes that may be classified, and those are high tide and low tide. The classification layer is the defined output layer that features these two tide classes. As opposed to this, the output size is two, and the cross-entropy is utilized as the loss function.

Batch normalization layer

Following the convolution, the output is normalized using a batch normalization layer, which improves training stability and speeds up convergence. This Table 2 has 69 layers, which are comprised of 1729 different convolution states. The original input image size is 227×227×3, and it is gradually decreased from 113×113×64 to 1×1×2 during the course of the subsequent process. The final step is the reduction of the classification result to 1×1×2 convolutions (Fig. 12).

Dataset loading phase

In order to train for tide detection, two main kinds of tide classes are used, with each class's high tide (104) and low tide (105) photos defining the training data size. A snapshot of the training dataset with two tide classes is shown in the Figure 13.

Training classes

The present comprises of two types of training results related to ResNet-18 and ResNet-50 i.e. training_validation_accuracy. The training dataset uses multi-layer deep convolution networks that contain5- pooling layers and 10-convolution layers, and 10-relu-convolution layers and used three types of most popular training optimizer algorithms such as root mean squared propagation (RMSProp), adaptive moment estimation (ADAM), stochastic gradient descent with momentum (SGDM)To find the best accuracy for the Tide disease dataset by varying epochs for aforesaid three algorithms and other training parameters is set to constant values such as sequence length is longest, sequence_padding_directionis 'right', minibatch size is 128, sequence_padding_valueis 0, squared_gradient_decay_factor is 0.9,

Table 2. ResNet-50 CNN layers (177)

S.No.	Name	Type	Activations (S × S ×C×B)	Learnable properties
1	Input_1image size 224×224×3 with ,zerocenter' normalization	Input image	224×224×3×1	
2	Conv1 [64 7×7×3] with stride [2 2] and padding [3 3 3 3]	Convolution	112×112×64×1	Weights (W) (7×7×3×64) and Bias (B) (1×1×64)
3	bn_conv1[64]	Branch Normalization	112×112×64×1	Offset 1 × 1 × 64 and Scale 1 × 1 × 64
4	Activation_1_relu	ReLu layer	112×112×64×1	
175	Fc1000	Fully connected	1×1×1000×1	W 1000 × 2048 and B 1000 × 1
176	Prob SoftMax	SoftMax	1×1×1000×1	
177	ClassificationLayer_fc1000 Crossentropyex with 'tench' and 999 other classes	Classification output	1×1×1000×1	

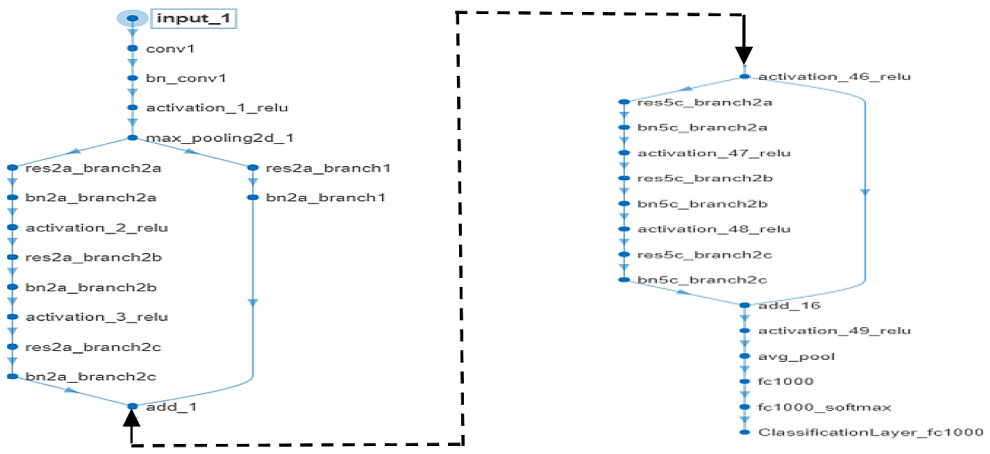

Figure 12. Deep learning ResNet-50 architecture

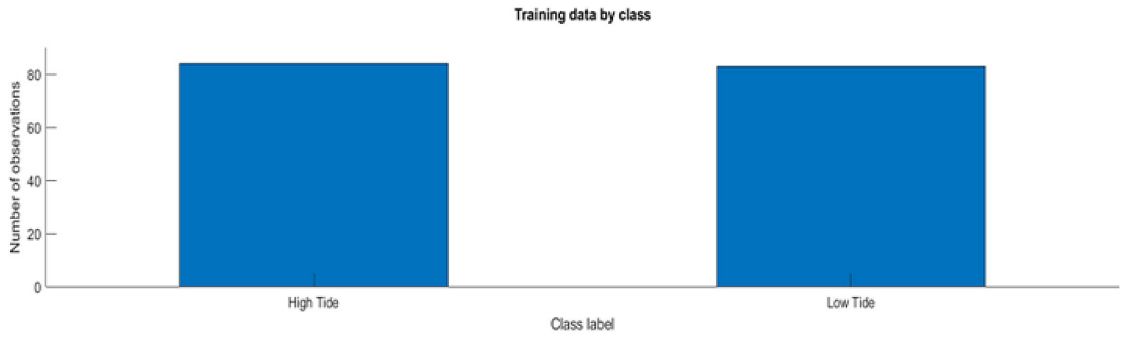

Figure 13. Screenshot of the tidal dataset with high tide and low tide classes

L2-regularizationis 0.0001, learn_rate_drop_factor is 0.1, learn_rate_drop_period is 10, epsilon is 1e-08, initial_learn_rate is 0.01. In addition, the gradient_thresholding_method is used to calculate the L2norms, where the distance of the vector coordinate from the origin of the vector space.

RESULTS AND DISCUSSION

According to the training results presented in Table 3, the training data attained 100% accuracy using the ResNet-18 and ResNet-50 architectures, contingent upon the previously defined parameters, with training accuracy varying based on the optimizer method and the number of epochs employed. Simulations indicated that the training dataset attained 100% accuracy in various scenarios, one utilizing the ADAM optimizer and the other employing RMSPROP.

Performance analysis of ResNet-18

The training results in Table 3 show that the ResNet-18 model reached 100% accuracy on the training data with our chosen settings. This performance varied depending on the choice of optimizer algorithm and the number of epochs. Interestingly, we observed that all three optimizers, ADAM and SGDM, achieved this peak accuracy. However, the RMSPROP optimizer failed to achieve 100% training accuracy, and peak training accuracy for RMSPROP is 98.61% at 50 epochs. Conversely, when applied to the ResNet-50 architecture on the same tide dataset, all three optimizers perform better and achieve 100% training accuracy. Upon further analysis, we found that the SGDM optimizer with ResNet-18 consistently achieved 98.61% accuracy across a range of epoch values from 50 to 500, with the exception of lower epochs, where we recorded 100% training accuracy. The ADAM optimizer demonstrated a distinct pattern, achieving lower accuracy (91.22% to 98.61%) at lower epochs (30 to 100) and achieving 100% at epoch 200. The overfitting problem caused the behavior to deteriorate after 200 epochs. Notably, SGDM emerged as the top performer, reaching the 100% accuracy mark in just 30 epochs and followed by the ADAM optimizer. The results suggest that using SDGM is preferable to training the tide dataset, if ResNet-18 is opted as deep learning training network. This performance variability across different epoch ranges and optimizers using ResNet-18 is clearly illustrated using gain and loss graphs in Figures 14–16, providing valuable insights into the optimization process for this particular tide dataset and model architecture.

Performance analysis of ResNet-50

The training results in Table 3 show that the ResNet-50 model reached 100% accuracy on the training data with our chosen settings. This performance varied depending on the choice of optimizer algorithm and the number of epochs. Interestingly, we observed that all three optimizers, ADAM and SGDM, achieved this peak accuracy. However, the RMSPROP optimizer failed to achieve 100% training accuracy, and peak training accuracy for RMSPROP is 100% at 75 epochs. After looking more closely, we found that the SGDM and ADAM optimizers with ResNet-50 always reached 100% accuracy for epochs ranging from 30 to 500. All three optimizers in the ResNet-50 network exhibit no overfitting problem. Whereas the performance of RMSPROP is similar to that of ResNet-18, except at epoch 75, where it achieved 100%, and the rest of the epochs, the accuracy ranges from 97.22% to 98.61%. Notably, SGDM and ADAM emerged as the top performers, reaching the 100% accuracy mark in just 30 epochs,

Table 3. Training data performance based on optimizer and epochs

Optimizer Algo.	Max_epochs	ResNet-18	ResNet-50
		Accuracy (%)	Accuracy (%)
SGDM	30	100	100
	40	100	100
	50	98.61	100
	75	98.61	100
	100	98.61	100
	200	98.61	100
	300	98.61	100
	400	98.61	100
	500	98.61	100
ADAM	30	91.22	100
	40	91.67	100
	50	93.06	100
	75	93.06	100
	100	98.61	100
	200	100	100
	300	95.83	100
	400	97.67	100
	500	97.22	100
RMSPROP	30	95.83	98.61
	40	95.83	98.61
	50	98.61	98.61
	75	97.22	100
	100	97.22	97.22
	200	91.67	97.22
	300	97.22	95.83
	400	95.83	97.22
	500	90.28	98.61

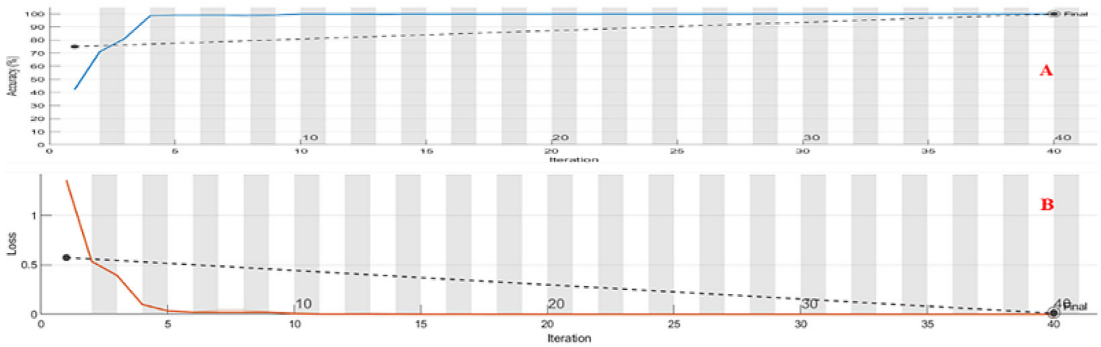

Figure 14. Attained 100% training accuracy test results using SGDM optimizer for ResNet-18 at Epochs-40 (A) gain graph and (B) loss graph

followed by the RMSPROP optimizer. If we use ResNet-50 as the deep learning training architecture, the training results suggest that using SDGM and ADAM is preferable to training the tide dataset. gain and loss graphs in Figures 17–19 clearly illustrate the performance variability across different epoch ranges and optimizers using ResNet-50, offering valuable insights into the optimization process for this specific tide dataset and model architecture.

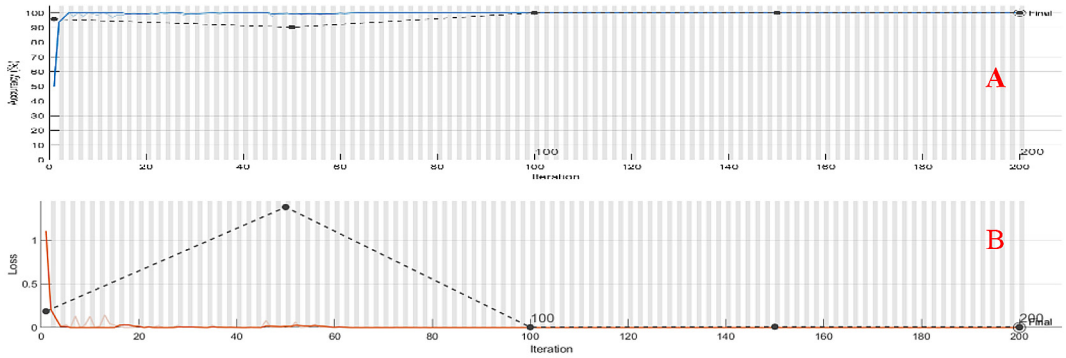

Figure 15. Attained 100% training accuracy test results using ADAM optimizer for ResNet-18 at Epochs-200 (A) gain graph and (B) loss graph

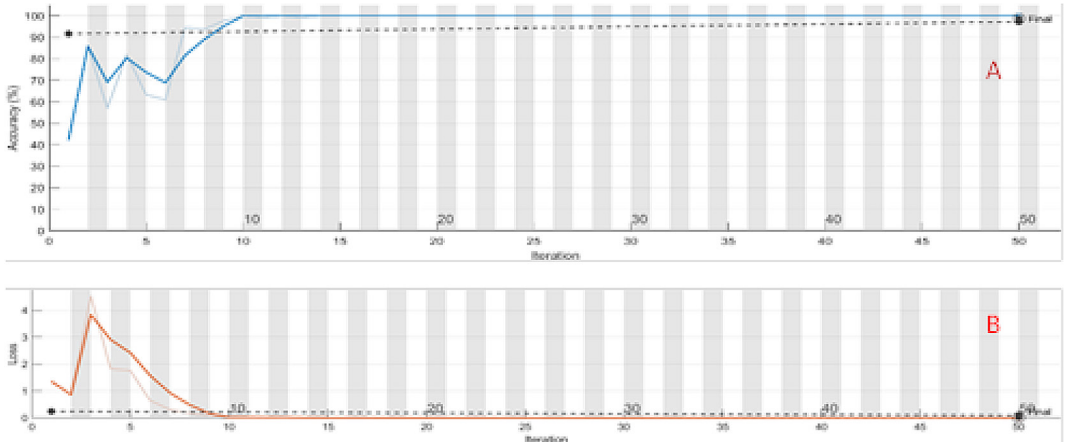

Figure 16. Attained 98.61% training accuracy test results using RMSPROP optimizer for ResNet-18 at Epochs-50 (A) gain graph and (B) loss graph

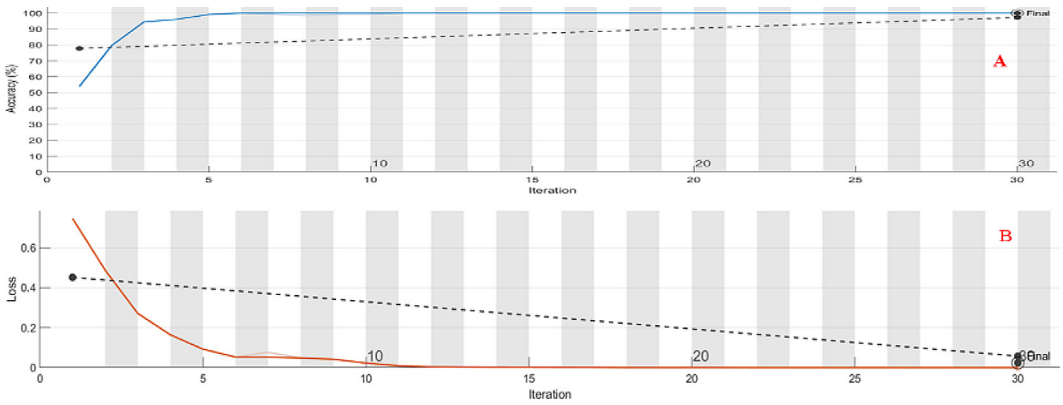

Figure 17. Attained 100% training accuracy test results using SGDM optimizer for ResNet-50 at Epochs-30 (A) gain graph and (B) loss graph

Performance comparison between ResNet-18 and ResNet-50

The training performance of ResNet-50 on the Tide dataset is comparatively higher than that of ResNet-18 in all three optimizers (Fig. 20). In particular, the performance of ResNet-18 reaches its peak in SGDM, with ADAM and RMSProp following closely behind (Table 3). All three optimizers performed poorly with ResNet-18. In most cases, the resultant accuracy of ResNet-18 remains consistently stable and low, regardless of the number of epochs, while the performance of ResNet-50 is improving at every Epoch that

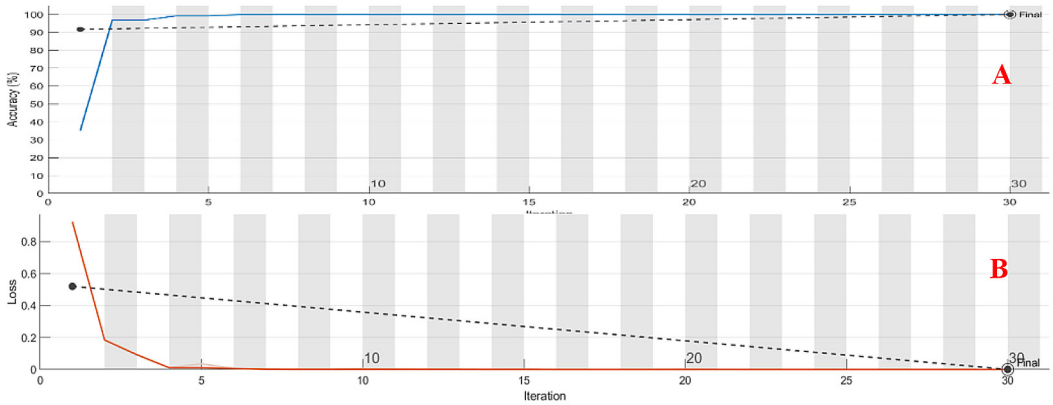

Figure 18. Attained 100% training accuracy test results using ADAM optimizer for ResNet-50 at Epochs-30 (A) gain graph and (B) loss graph

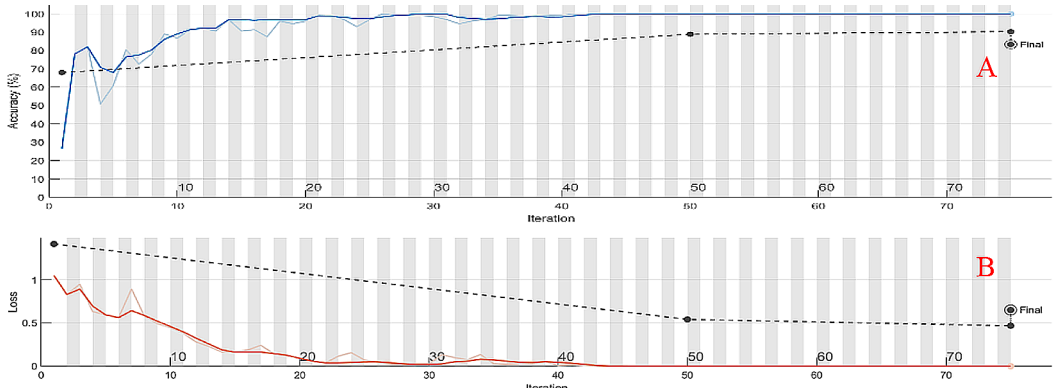

Figure 19. Attained 100% training accuracy test results using RMSPROP optimizer for ResNet-50 at Epochs-75 (A) gain graph and (B) loss graph

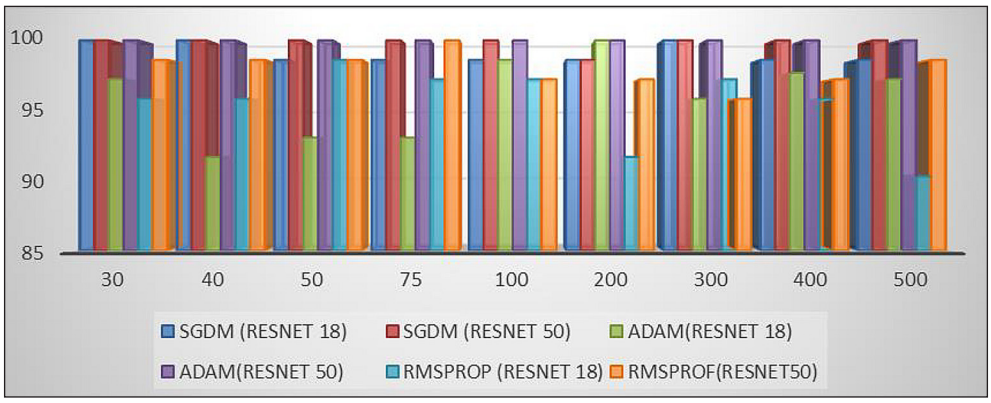

Figure 20. Performance analysis of ResNet-18 and ResNet-50 on SGDM, ADAM and RSMPROP optimizers on tidal dataset against epochs

exhibits varying accuracies across the three optimizers. We have observed that the SDGM optimizer's training accuracy for ResNet-18 varied according to Epochs, whenever the lower Epochs are used the accuracy is lower i.e., 90.28% at 500 epoch and 100% at 30 and peak performance is observed both deep learning training architectures remains constant. However, when the Epochs are varied from 30 to 500 while keeping other tuning parameters like learning rate and batch size constant, the performance of the ADAM and RMSPROP optimizers also varied but recorded lower accuracies compared with SGDM. The ResNet-18 dataset's training is faster than that of

ResNet-50, with ResNet-50 requiring nearly five times more resources to train the current custom dataset. For the tide dataset, ResNet-18 executes quickly and has a training accuracy that is 2.72% lesser than ResNet-50 (Fig. 21).

Compared to ResNet-18, the average dataset training performance of ResNet-50 using SGDM is high, but only ResNet-18 exhibits peak performance. Almost the majority of optimizers show a stable performance with minor differences in both the ResNet-18 and ResNet-50 models. In ResNet-18, the average performance of RMSPROP is high at 35%, followed by SGDM (33%) and ADAM (32%), as shown in figure 21. Using SGDM results in 38% lower performance for ResNet-50, followed by 32% for ADAM and 30% for RMSPROP. ResNet-50 performed much better than ResNet-18 because it used depthwise separable convolutions, which cut down on the number of parameters and the cost of computing them.

DISCUSSION

The current experiment suggests that ResNet-50 deep learning networks train the Tide dataset for higher accuracy. Similar research was proposed by Ashhar et al. (2021), who mostly looked at how well different deep learning models, like GoogleNet, SqueezeNet, DenseNet, ShuffleNet, and MobileNetV2, could classify lung cancers shown on CT scans. But their research didn't use the Tide dataset and considered medical CT scan images as input. Detection of high and low tides from the images is very complex compared with the medical CT scan images due to [Ashhar et al. 2021]. In addition, their research was not considered the hyper tuning of training parameters like optimizers like SGDM, ADAM and RMSProp with a change in the epochs size. Both Optimizers and epochs plays a crucial role for higher training accuracy, the current results already proved it with 100% accurate, while their research obtained a maximum training accuracy of 94.13% by SqueezNet. So, from the present research we suggest that selection of right optimizers and epochs will make difference in the training accuracy. The size of the dataset is another important aspect for the performance measure of the deep training model. Yahya et al. (2021) have implemented a transfer learning approach, utilizing five different networks, to detect face masks and mitigate the impact of Covid-19 on the public. For mask data training, they mostly used AlexNet, GoogleNet, ResNet-18, ResNet-50, and ResNet-101. AlexNet had a 95% success rate at constant epochs when they used a standard optimizer. But their research varied the size of the dataset training initially from 20 images to 400 with a random interval, but their research has not discussed whether the dataset is balanced or imbalanced. In addition, the mask object detection is easy compared with the tide detection due to the fragile structure of the tide image [Yahya et al., 2021]. Our research suggests that hyper-tuning training parameters, rather than changing the dataset for higher accuracy, is a better option. Working with a larger dataset, the computation time also increases compared with a smaller dataset. The present work used only 209 images to achieve higher accuracy.

Detection of uncertain objects, which represent the fragile objects, is always a challenging task compared with the static image objects. Dahiya et al. (2022) looked for a way to train a system to recognize standard objects from three species,

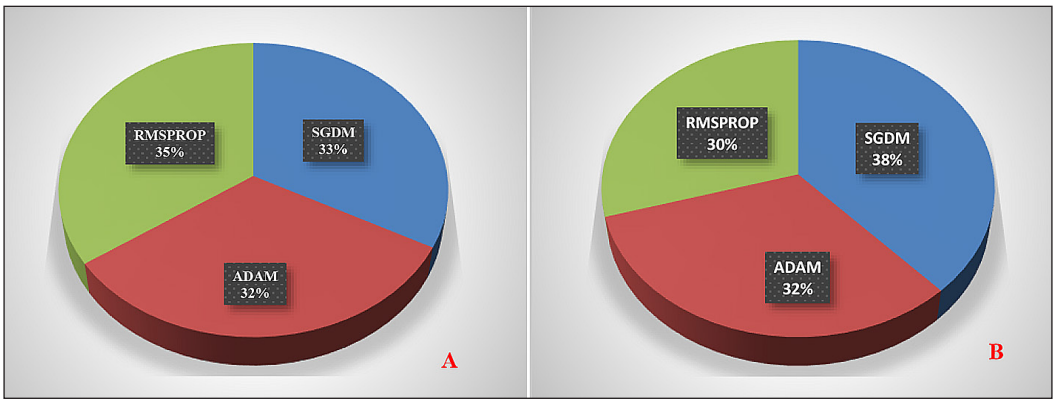

Figure 21. Distribution chart of optimizers performance using (A) ResNet-18 training network; (B) ResNet-50 on tidal dataset

like a tomato, pepper, or potato. They used a dataset of 20,640 photos and 15 different classifications. They studied training accuracy and used eight different deep learning architectures to train the dataset: AlexNet, GoogleNet, MobileNet, ResNet-18, ResNet-50, ResNet-101, ShuffleNet, and SqueezeNet. The hyperparameters employed included epochs, learning rate, batch size, and optimizer for higher accuracies. Even their research focused on static objects and did not address issues with fragile objects, like tide detection. But the current research focused on tide detection and found the best training network for the fragile objects like high and low tides [Dahiya et al., 2022].

The deep learning procedures were applied to public safety applications, like road breaking identifications and resulted with high accuracy using AlexNet, ResNet18, and SqueezeNet on 4333 image dataset of roads. Even they addressed the training issues for road dataset, but did'nt mentioned on ResNet-50 architecture, especially for fragile and uncertain object detection. But the proposed research well focused on the training issues for the uncertain objects by addressing the public safety parameter into concern. In addition the selection of optimizers are also missing from their discussion. This work also concentrated on optimizers in addition to epochs, that made a clear difference in aching the higher accuracies for smaller epochs [Ullah et al. 2022].

As specified in the above the selection of optimizers is a major concern in the deep learning traning datset task. Kumar et al. (2023) accuracy results are 94.99%, 94.61%, and 94.09% were attained, respectively, through hyper-parameter optimization utilizing flood data. According on the detection analysis findings, AlexNet outperforms both GoogleNet and SqueezeNet. We accomplished this by fine-tuning hyper-parameters, with particular focus on optimizers such as ADAM, SGDM, and RMSProp w.r.t. ResNet-18 and ResNet-50 models and obtained 100% training accuracy in both, whereas in their experimentation the Google Net model facilitated an accuracy of 94.53%, according to [Kumar et al., 2023]. They employed epochs, learning rate, small batch size, and optimizer as parameters for the model; however, their study has not addressed the challenges associated with the tide datasets. Their Epoch range spans from thirty to fifty, employing exclusively the ADAM and SGDM optimizers. The RMSProp optimizer is not utilized. The Epochs have been altered from 30 to 500 in the current study, however. Among the eight deep learning architectures, only Google Net has superior performance in continuously detecting larger datasets. They can accommodate a maximum of two optimizers and function for up to three epochs. Three separate optimizer types – SGDM, ADAM, and RMSProp – were employed throughout six different epochs, varying in duration from thrity to five hundred, in the current study. In our previous works we performed analogous investigations on flood object training challenges associated with AlexNet and XceptionNet, although did not address ResNet training concerns [Lambu et al., 2024]. In addition the present research is more focused on the fragile objects like tide detection in the beaches. The latest study may assist researchers managing smaller datasets by enabling them to effectively adjust hyperparameters and achieve improved accuracy. Most deep learning detection techniques are evaluated on datasets pertaining to agriculture and medical. This study is novel since it employs a private collection of photographs affected by beach tides to ascertain high-tide levels on Indian beaches, ranging from 0.96 m to 1.83 m. High-tide early detection via deep learning offers the coast guard critical information to advise beach swimmers for safety and rescue operations.

CONCLUSIONS

The present investigation has achieved the study's objectives. The research identifies the optimal deep-learning network for the effective training of tide object data. The study demonstrates that the SGDM optimizer is the most effective method for training tide object datasets, yielding higher detection accuracies. The training accuracy results indicate that lower epoch rates correlate with reduced accuracies for the tide object dataset, necessitating median Epoch rates of at least 30 to 500 to attain higher accuracies. The research advises against the utilization of SGDM and ADAM optimizers for training tide object datasets. Analysis of the observed data indicates that training tide object datasets using ResNet-50 and the SGDM optimizer for epochs ranging from 30 to 500 yields improved outcomes. These studies aid researchers in adhering to recommended Epochs for training tide object datasets, as selecting the appropriate optimizer can decrease training time and potentially enhance both training and

testing accuracies. This research provides a valuable resource for training tide objects affected by high tides resulting from rip currents, which are significant in the context of climate change and rising sea levels. This research focuses exclusively on the training challenges related to high-tide and low-tide object datasets. Additionally, it is essential to conduct accuracy evaluations of the research using detector algorithms including RCNN, YOLO, and Mobile Net. The outcomes of this research significantly recommend ResNet-50 deep learning training for the identification of high tides for beach areas over ResNet-18. Even ResNet-18 executes quickly, but still ResNet-50 gives best training classification accuracy.

REFERENCES

1. Almar, R., Marchesiello, P., Almeida, L.P., Thuan, D.H., Tanaka, H. & Viet, N.T. (2017). Shoreline response to a sequence of typhoon and monsoon events. *Water, 9*(6), 364. https://doi.org/10.3390/w9060364
2. Ashhar, S.M., Mokri, S.S., Abd Rahni, A.A., Huddin, A.B., Zulkarnain, N., Azmi, N.A. & Mahaletchumy, T. (2021). Comparison of deep learning convolutional neural network (CNN) architectures for CT lung cancer classification. *International Journal of Advanced Technology and Engineering Exploration, 8*(74), 126. http://dx.doi.org/10.19101/IJATEE.2020.S1762126.
3. Dahiya, S., Gulati, T. & Gupta, D. (2022). Performance analysis of deep learning architectures for plant leaves disease detection. *Measurement: Sensors, 24*, 100581. https://doi.org/10.1016/j.measen.2022.100581
4. de Silva, A., Mori, I., Dusek, G., Davis, J. & Pang, A. (2021). Automated rip current detection with region based convolutional neural networks. *Coastal Engineering, 166*, 103859. https://doi.org/10.1016/j.coastaleng.2021.103859
5. George, E., Smith, A., O'Rourke, C., Cherry, N., Sfalcin, A. & Houser, C. (2024). Citizen science monitoring of beach and dune erosion during Hurricane Fiona. *Physical Geography*,1–20. https://doi.org/10.1080/02723646.2024.2324516
6. Girin, T., Lejay, L., Wirth, J., Widiez, T., Palenchar, P.M., Nazoa, P., Touraine, B., Gojon, A. & Lepetit, M. (2007). Identification of a 150 bp cis-acting element of the AtNRT2. 1 promoter involved in the regulation of gene expression by the N and C status of the plant. *Plant, Cell & Environment*, *30*(11), 1366–1380. https://doi.org/10.1111/j.1365-3040.2007.01712
7. Halliday, G.M., Holton, J.L., Revesz, T. & Dickson, D.W. (2011). Neuropathology underlying clinical variability in patients with synucleinopathies. *Acta Neuropathologica*, 122, 187–204. https://doi.org/10.1007/s00401-011-0852-9
8. Koon, W., Brander, R.W., Dusek, G., Castelle, B. & Lawes, J.C. (2023). Relationships between the tide and fatal drowning at surf beaches in New South Wales, Australia: Implications for coastal safety management and practice. *Ocean & Coastal Management, 238*, 106584. https://doi.org/10.1016/j.ocecoaman.2023.106584
9. Kumar V., Azamathulla H. M, Sharma K. V, Mehta D. J, & Maharaj K. T. (2023). The state of the art in deep learning applications, challenges, and future prospects: A comprehensive review of flood forecasting and management. *Sustainability*, *15*(13), 10543. https://doi.org/10.3390/su151310543
10. Kumar, T., Brennan, R., Mileo, A. & Bendechache, M. (2024). Image data augmentation approaches: A comprehensive survey and future directions. *IEEE Access,* 12, 187536–187571. https://doi.org/10.1109/ACCESS.2024.3470122
11. Lambu, P. & Duvvuru, R. (2024). Training Issues in Classifying Seashore tide Object Detection–A Deep Learning Study. *Ecological Engineering & Environmental Technology, 25*(10). https://doi.org/10.12912/27197050/191861
12. Lange, M., Joly, F., Vardy, J., Ahles, T., Dubois, M., Tron, L., Winocur, G., De Ruiter, M.B. & Castel, H. (2019). Cancer-related cognitive impairment: an update on state of the art, detection, and management strategies in cancer survivors. *Annals of Oncology*, *30*(12), 1925–1940. https://doi.org/10.1093/annonc/mdz410
13. Li, G., Yang, Y., Qu, X., Cao, D. & Li, K. (2021). A deep learning based image enhancement approach for autonomous driving at night. *Knowledge-Based Systems*, *213*, 106617. https://doi.org/10.1016/j.knosys.2020.106617
14. Little, M., Rosa, E., Heasley, C., Asif, A., Dodd, W. & Richter, A. (2022). Promoting healthy food access and nutrition in primary care: a systematic scoping review of food prescription programs. *American Journal of Health Promotion, 36*(3), 518–536. https://doi.org/10.1177/08901171211056584
15. Liu, H., Li, C., Wu, Q. & Lee, Y.J. (2024). Visual instruction tuning. *Advances n Neural Information Processing Systems*, 36. https://doi.org/10.1016/j.knosys.2020.106617.
16. Mazloomzadeh, S., Khaleghparast, S., Ghadrdoost, B., Mousavizadeh, M., Baay, M.R., Noohi, F., Sharifnia, H., Ahmadi, A., Tavan, S., Alamdari, N.M. & Fathi, M. (2021). Effect of intermediate-dose vs standard-dose prophylactic anticoagulation on thrombotic events, extracorporeal membrane

oxygenation treatment, or mortality among patients with COVID-19 admitted to the intensive care unit: *the INSPIRATION randomized clinical trial. Jama, 325*(16), 1620–1630. https://doi.org/10.1001/jama.2021.4152

17. Mehta, L., Srivastava, S., Adam, H.N., Alankar, Bose, S., Ghosh, U. & Kumar, V.V. (2019). Climate change and uncertainty from 'above' and 'below': perspectives from India. *Regional Environmental Change*, *19*, 1533–1547.
18. Meliboev, A., Alikhanov, J. & Kim, W. (2022). Performance evaluation of deep learning based network intrusion detection system across multiple balanced and imbalanced datasets. *Electronics, 11*(4), 515. https://doi.org/10.3390/electronics11040515
19. Mohana, A.A., Farhad, S.M., Haque, N. & Pramanik, B.K. (2021). Understanding the fate of nano-plastics in wastewater treatment plants and their removal using membrane processes. *Chemosphere, 284*, 131430. https://doi.org/10.1016/j.chemosphere.2021.131430
20. Najafzadeh, M., Basirian, S. & Li, Z. (2024). Vulnerability of the rip current phenomenon in marine environments using machine learning models. *Results in Engineering, 21*, 101704. https://doi.org/10.1016/j.rineng.2023.101704
21. Pikelj, K., Ružić, I., Ilić, S., James, M.R. & Kordić, B. (2018). Implementing an efficient beach erosion monitoring system for coastal management in Croatia. *Ocean and Coastal Management, 156*, 223–238. https://doi.org/10.1016/j.ocecoaman.2017.11.019
22. Puleo, J.A., Lanckriet, T., Conley, D. & Foster, D. (2016). Sediment transport partitioning in the swash zone of a large-scale laboratory beach. *Coastal Engineering, 113*, 73–87. https://doi.org/10.1016/j.coastaleng.2015.11.001
23. Ramakrishna, C.R. & Sivaperuman, C. (2010). Biodiversity of Andaman and Nicobar Islands–an overview. *Recent trends in biodiversity of Andaman, Nicobar Islands. Zoological Survey of India, Kolkata,*1–42.
24. Ravimuni, K. & Rani, K.U. (2022). Demographic Profile of Deaths Due to Drowning in and Around Vijayawada, Andhra Pradesh. *Indian Journal of Forensic Medicine & Toxicology*, *16*(1). https://doi.org/0.37506/ijfmt.v16i1.17571
25. Ray-Bennett, N.S., Dissanayake, L., Ekezie, W., Macleod, L., Mecrow, T., Saunders, C., Sindall, R., Oporia, F. & Rahman, A. (2024). How drowning data is collected in low-and middle-income countries (LMICs): A scoping review. *Injury Prevention*, *30*, A131-A132 https://doi.org/10.1136/injuryprev-2024-SAFETY.314
26. Shimada, R., Ishikawa, T., Toguchi, H. & Komine, T. (2023). Study on appropriate time interval of image averaging for rip current detection. In: International Conference on Asian and Pacific Coasts. 1135–1144. Singapore: Springer Nature Singapore. https://doi.org/10.1007/978-981-99-7409-2_103
27. Ullah, A., Elahi, H., Sun, Z., Khatoon, A. & Ahmad, I. (2022). Comparative analysis of AlexNet, ResNet18 and SqueezeNet with diverse modification and arduous implementation. *Arabian Journal for Science and Engineering, 47*(2), 2397–2417.
28. Vitousek, S., Buscombe, D., Vos, K., Barnard, P.L., Ritchie, A.C. & Warrick, J.A. (2023). The future of coastal monitoring through satellite remote sensing. *Cambridge Prisms: Coastal Futures, 1*(10). https://doi.org/10.1017/cft.2022.4
29. Yadhunath, E.M., Seelam, J.K. & Jishad, M. (2022). Rip current occurrences in meso tidal surf zones at a coastal stretch along the central west coast of India. *Regional Studies in Marine Science*, 51, 102180. https://doi.org/10.1016/j.rsma.2022.102180
30. Yahya, S.N., Ramli, A.F., Nordin, M.N., Basarudin, H. & Abu, M.A. (2021). Comparison of convolutional neural network architectures for face mask detection. *International Journal of Advanced Computer Science and Applications*, *12*(12), 667–677.